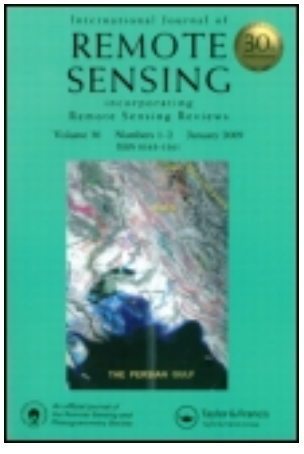

International Journal of Remote Sensing

Publication details, including instructions for authors and subscription information:
http://www.tandfonline.com/loi/tres20

Using AHS hyper-spectral images to study forest vegetation recovery after a fire

Margarita Huesca [a], Silvia Merino-de-Miguel [b], Federico González-Alonso [c], Sergio Martínez [d], José Miguel Cuevas [c] & Abel Calle [e]

[a] ETSI Montes, Universidad Politécnica de Madrid, 28040, Madrid, Spain

[b] EUIT Forestal, Universidad Politécnica de Madrid, 28040, Madrid, Spain

[c] Remote Sensing Laboratory, CIFOR - INIA, Madrid, 28040, Spain

[d] Consejería de Medio Ambiente y Desarrollo Rural, Junta de Castilla-La Mancha, Toledo, Spain

[e] Departamento de Física Aplicada, Universidad de Valladolid, 47002 Valladolid, Spain

Version of record first published: 25 Feb 2013.

To cite this article: Margarita Huesca , Silvia Merino-de-Miguel , Federico González-Alonso , Sergio Martínez , José Miguel Cuevas & Abel Calle (2013): Using AHS hyper-spectral images to study forest vegetation recovery after a fire, International Journal of Remote Sensing, 34:11, 4025-4048

To link to this article: http://dx.doi.org/10.1080/01431161.2013.772313

International Journal of Remote Sensing, 2013
Vol. 34, No. 11, 4025–4048, http://dx.doi.org/10.1080/01431161.2013.772313

Using AHS hyper-spectral images to study forest vegetation recovery after a fire

Margarita Huesca[a], Silvia Merino-de-Miguel[b]*, Federico González-Alonso[c], Sergio Martínez[d], José Miguel Cuevas[c], and Abel Calle[e]

[a]ETSI Montes, Universidad Politécnica de Madrid, 28040 Madrid, Spain; [b]EUIT Forestal, Universidad Politécnica de Madrid, 28040 Madrid, Spain; [c]Remote Sensing Laboratory, CIFOR – INIA, Madrid, 28040 Spain; [d]Consejería de Medio Ambiente y Desarrollo Rural, Junta de Castilla-La Mancha, Toledo, Spain; [e]Departamento de Física Aplicada, Universidad de Valladolid, 47002 Valladolid, Spain

(*Received 30 November 2010; accepted 5 January 2013*)

Recent advances in sensor technology have led to the development of new hyper-spectral instruments capable of measuring reflected radiation over a wide range of wavelengths. These instruments can be used to assess the diverse characteristics of vegetation recovery that are only noticeable in certain parts of the electromagnetic spectrum. In this research, such instruments were used to study vegetation recovery following a forest fire in a Mediterranean ecosystem. The specific event occurred in an area called El Rodenal of Guadalajara (in Central Spain) between 16 and 21 July 2005. Remotely sensed hyper-spectral multitemporal data were used to assess the forest vegetation response following the fire. These data were also combined with remotely sensed fire severity data and satellite high temporal resolution data. Four Airborne Hyperspectral Scanner (AHS) hyper-spectral images, 361 Moderate Resolution Imaging Spectroradiometer (MODIS) images, field data, and ancillary information were used in the analysis. The total burned area was estimated to be 129.4 km^2. AHS-derived fire severity level-of–damage assessments were estimated using the normalized burn ratio (NBR). Post-fire vegetation recovery was assessed according to a spectral unmixing analysis of the AHS hyper-spectral images and the normalized difference vegetation index (NDVI), as calculated from the MODIS time series. Combining AHS hyper-spectral images with field data provides reliable estimates of burned areas and fire severity levels-of-damage. This combination can also be used to monitor post-fire vegetation recovery trends. MODIS time series were used to determine the types and rates of vegetation recovery after the fire and to support the AHS-based estimates. Data and maps derived using this method may be useful for locating priority intervention areas and planning forest restoration projects.

1. Introduction

Each year, wildfires affect millions of hectares of forests worldwide. Fires release a significant amount of greenhouse gases, particulates, and aerosol emissions into the atmosphere, and these emissions significantly alter the chemistry of the atmosphere (Chuvieco 2009). Global estimates of total gas emissions from biomass burning are uncertain (Palacios-Orueta et al. 2005); according to studies, the total may range between 2.0 Pg C year^{-1}

*Corresponding author. Email: silvia.merino@upm.es

(Van der Werf et al. 2010) and 4.5 Pg C year^{-1} (Levine 1996). At regional and local scales, fires also affect vegetation composition; landscape structure, composition, and function; biodiversity; soil erosion; air quality; and the water cycle; and they have important impacts on human health, lives, and properties (Díaz-Delgado, Lloret, and Pons 2003; Lentile et al. 2006; Röder et al. 2008; Chuvieco 2009). Fires change the composition of the atmosphere and land-use patterns, but they are also affected by these processes (Chuvieco 2009). Previous management practices and global warming may increase the frequency and severity of wildfires (Levine 1991; van Leeuwen et al. 2010). This is especially important in the Mediterranean region, where fire is no longer a natural ecological issue but rather a persistent and common anthropogenic impact (Pérez-Cabello et al. 2009). According to Pausas (2004), if the current climatic trends of increasing annual and summer temperatures and decreasing summer rainfall continue, fuels will become drier, which will, in turn, increase the risk of fire for large areas (Pausas 2004) and amplify the hazard of desertification (Moreno 2007).

The effects of fire on vegetation are related to the susceptibility of plants to heat and flames (Pérez-Cabello et al. 2009). In the Mediterranean region, many species exhibit either passive defence (e.g. thick bark) or active regeneration mechanisms (e.g. seed production, seed banking, and sprouting) to rapidly overcome the effects of fire (Mooney and Hobbs 1986). However, over the long term, fire may change vegetation composition and landscape patterns (Pérez-Cabello et al. 2009), threatening the persistence of species less adapted to fire. The post-fire response of many types of vegetation is largely variable because it is influenced by structural (e.g. altitude, slope, and aspect; soil type and condition; land-use patterns; vegetation composition and status) and temporal (e.g. burn severity; post-fire temperature and rainfall; post-fire management) factors (Retana et al. 2002; Díaz-Delgado, Lloret, and Pons 2003; Pausas, Ribeiro, and Vallejo 2004; Röder et al. 2008; van Leeuwen 2008; Pérez-Cabello et al. 2009).

Land managers attempt to identify areas where poor post-fire regeneration is expected to plan future restoration projects (Pausas, Ribeiro, and Vallejo 2004). Remotely sensed optical images enable managers to identify priority intervention areas (Ruíz-Gallardo, Castaño, and Calera 2004; Lentile et al. 2006) and to study long-term vegetation recovery (Röder et al. 2008; Vicente-Serrano, Pérez-Cabello, and Lasanta 2008; Pérez-Cabello et al. 2009). Remote-sensing data are particularly appropriate for the latter task because of their capacity to reflect slight changes on the land surface and their high spatial and temporal resolutions (Lentile et al. 2006). Studies of post-fire vegetation recovery using satellite data have been used to document regeneration rates (Lentile et al. 2006; Röder et al. 2008), explore the influence of structural and temporal factors (Díaz-Delgado, Lloret, and Pons 2003; Röder et al. 2008; van Leeuwen et al. 2010), and study vegetation response in relation to burn severity (Díaz-Delgado, Lloret, and Pons 2003; Ruíz-Gallardo, Castaño, and Calera 2004). The majority of these assessments have been conducted using medium to high spatial resolution multispectral data (e.g. Landsat MSS (Multispectral Scanner), TM (Thematic Mapper), and ETM+ (Enhanced Thematic Mapper Plus)) (Viedma et al. 1997; Díaz-Delgado, Lloret, and Pons 2003; Vicente-Serrano, Pérez-Cabello, and Lasanta 2008), although hyper-spectral images have also been used (Riaño et al. 2002; Kokaly et al. 2007). Most studies have relied on spectral vegetation indices such as the NDVI (normalized difference vegetation index) (Viedma et al. 1997; Díaz-Delgado, Lloret, and Pons 2003; Vicente-Serrano, Pérez-Cabello, and Lasanta 2008), which measures direct changes in the green vegetation cover (Lentile et al. 2006), while others have used techniques such as principal component analysis, Kauth–Thomas transformation, and spectral mixture analysis (Lentile et al. 2009; Pérez-Cabello et al. 2009).

Spectral mixture analysis (SMA; common synonyms: linear spectral unmixing, mixture modelling, linear model for signal mixing) is particularly useful in post-fire vegetation recovery studies in the Mediterranean context (Röder et al. 2008). This technique, which relies on the assumptions of linear spectral mixing models (Settle and Drake 1993; Drake, Mackin, and Settle 1999), can be applied to any type of imagery with multiple reflectance channels, including both multispectral and hyper-spectral data sets (Lentile et al. 2009). It estimates the surface abundance of several pure spectral components (referred to as endmembers), which together produce the observed mixed spectral signature of the pixel (Cochrane and Souza 1998; González-Alonso et al. 2007). In this case, the limitation of having fewer components than bands must be considered. The intrinsic dimensionality of the spectral data rather than the number of spectral bands should be utilized (Settle and Drake 1993).

Several studies have stressed the need for long-term post-fire ecosystem monitoring (van Leeuwen et al. 2010). The majority of remote-sensing assessments of post-fire vegetation response are based on multitemporal Landsat imagery (Viedma et al. 1997; Miller and Yool 2002; Díaz-Delgado, Lloret, and Pons 2003; Lentile et al. 2006; Röder et al. 2008; Vicente-Serrano, Pérez-Cabello, and Lasanta 2008). Researchers working with Landsat data have developed appropriate radiometric correction techniques because multitemporal data sets, particularly those compounded by Landsat images, are affected by different sources of noise, which, in turn, complicates analyses of the results (Röder et al. 2008; Vicente-Serrano, Pérez-Cabello, and Lasanta 2008). Only a limited number of studies have used high temporal resolution data sets, such as those provided by the MODIS (Moderate Resolution Imaging Spectroradiometer) sensor. According to van Leeuwen (2008), MODIS NDVI time-series data are a 'valuable resource to detect trends, seasonality, and anomalies in forest vegetation dynamics that are changing due to wildfire'. Van Leeuwen et al. (2010) successfully monitored post-fire vegetation response in three dry land ecosystems using MODIS NDVI time-series data (16-day composite, 250-m pixel resolution) for the period of 2000–2007.

Accurate information on the impacts of fire (fire and burn severity) can provide a baseline for monitoring landscape response to fire (van Leeuwen 2008). Fire severity, which integrates physical, chemical, and biological changes caused by fire (White et al. 1996), is usually estimated from remote-sensing data because this is the only cost-effective and efficient approach for gathering post-fire information (Gitas, de Santis, and Mitri 2009). Several researchers have shown a direct positive relationship between fire severity and post-fire regeneration response (Díaz-Delgado, Lloret, and Pons 2003; Lentile et al. 2006), indicating the importance of including such attributes in vegetation recovery studies. Fire severity studies have mainly used medium to high spatial resolution images, such as Landsat-TM and -ETM+, Envisat-MERIS (Medium Resolution Imaging Spectrometer), and SPOT (Système Pour l'Observation de la Terre) (Roldán-Zamarrón et al. 2006; Miller and Thode 2007; De Santis and Chuvieco 2007; González-Alonso et al. 2007). Standard fire severity maps classify territories into categories of unburned, low, moderate, and high damage based on spectral vegetation indices or classification schemes (Lentile et al. 2006; Lewis et al. 2007). The normalized burn ratio (NBR) index effectively identifies areas affected by fire and accurately evaluates burn severity (Cocke, Fulé, and Crouse 2005; Wimberly and Reilly 2007; Vicente-Serrano, Pérez-Cabello, and Lasanta 2008; Gitas, de Santis, and Mitri 2009), although this approach has not always performed optimally (Roy, Boschetti, and Trigg 2006).

The primary goal of this research was to evaluate the effectiveness and usefulness of remotely sensed hyper-spectral multitemporal data for assessing post-fire forest vegetation

response in a Mediterranean ecosystem. The following secondary objectives were also identified: (i) to explore the ability of remotely sensed hyper-spectral data to produce a fire severity map rapidly and cost-effectively; (ii) to examine the medium-term (3 years) influence of fire severity on post-fire vegetation response; and (iii) to evaluate the use of high temporal resolution MODIS NDVI time-series data to monitor post-fire forest vegetation response and to complement hyper-spectral data sets with high spatial and spectral resolutions.

2. Study area

The study area is located in the northeastern part of Guadalajara province (Central Spain) in an area called El Rodenal (Figure 1), where a forest fire occurred between 16 and 21 July 2005. The fire started in an area called Cueva de Casares (Riba de Saelices municipality) from a barbecue and rapidly spread due to adverse weather conditions, including a high temperature of 35°C, a low relative humidity of 22%, 30 days since the last rainfall event, and moderate to high wind speeds from 10 to 23 km h^{-1} (De Santis and Chuvieco 2007). The fire lasted 5 days, killed 11 fire-fighters, and burned a total of 130 km^2 of forest dominated by *Pinus pinaster* with an understory of *Quercus pyrenaica* and *Quercus faginea* and bushes of *Cistus* sp., *Cytisus* sp., and *Erica* sp. The area was characterized by a spatially connected supply of fuel, an essential factor for fire propagation. A portion of the affected area (roughly 31.5 km^2) was located within the limits of the Alto Tajo Natural Park. The affected area has a complicated topography, with altitudes ranging between 1100 and 1400 m, and is characterized by a network of deep valleys with steep gradients. From a geological perspective, the study area is a sequence of limestone and sandstone deposits, and the main types of soils are Xerochrept, Plexeralf, and Xerorthent (De Santis and Chuvieco 2007). Rainfall in the region averages 500 mm per year, with maximum values at the end of autumn and minimum values during summer. The average annual temperature is 10.5°C.

3. Material

3.1. Hyper-spectral AHS images

The Remote Sensing Laboratory of CIFOR-INIA (Forest Research Centre – National Institute for Agricultural Research, Spain) owns a set of four hyper-spectral images of the study area (Figure 1), one per year between 2005 and 2008. These images were acquired by

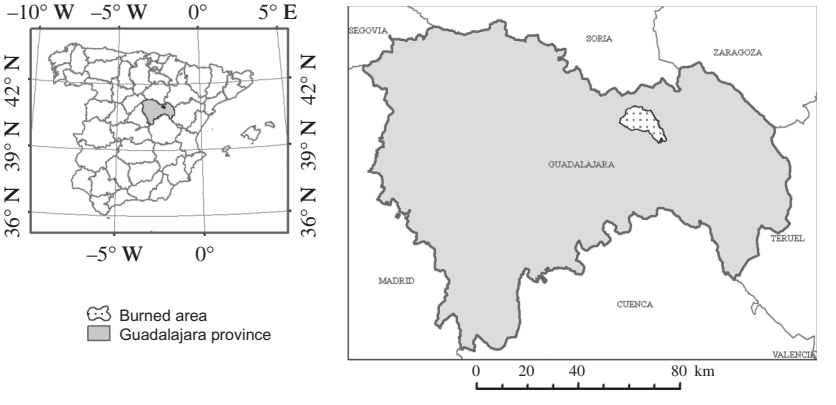

Figure 1. Study area in Guadalajara province, central Spain.

the AHS (Airborne Hyperspectral Scanner) sensor that flies on-board a CASA-C212 aeroplane. Hyper-spectral images were used to assess fire severity and to monitor post-fire vegetation regeneration.

The AHS sensor is an 80-band airborne imaging radiometer, developed by ArgonST (USA) and operated by INTA (National Institute for Aerospace Technology, Spain) since 2004. It has 63 bands in the reflective part of the spectrum (430–2500 nm), seven bands in the middle-infrared region (3300–5400 nm), and 10 bands in the thermal infrared region (8200–12,700 nm). The AHS sensor is a line-scanner with an FOV (field of view) of 90°, an IFOV (instantaneous field of view) of 3.5 mrad, and an average spatial resolution of 3 m. Once energy coming from the earth reaches the sensor, it is divided into five optical ports: PORT1, PORT2A, PORT2, PORT3, and PORT4. Each port corresponds to one of the following spectral regions: VIS (visible), NIR (near-infrared), SWIR (shortwave infrared), MIR (middle-infrared), and TIR (thermal infrared). Bandwidths vary according to the spectral region. Information is coded in 12 bits, and each line in an image is compounded by 750 pixels. AHS accounts for two internal sources of reference, both of which are black bodies of selectable temperature. These two black objects are sensed with every new line, proving zero radiance values for the reflective channels (PORT1, PORT2A, and PORT2) and calibration levels for the emissive bands (PORT3 and PORT4).

The first image was acquired on 6 October 2005, a few weeks after the fire and just before the first autumn rainfalls. This image clearly reflects the state of the vegetation cover after the fire. Three additional flights were conducted in 2006 (6 October), 2007 (28 September), and 2008 (15 September) (Figure 2). Each campaign consisted of seven

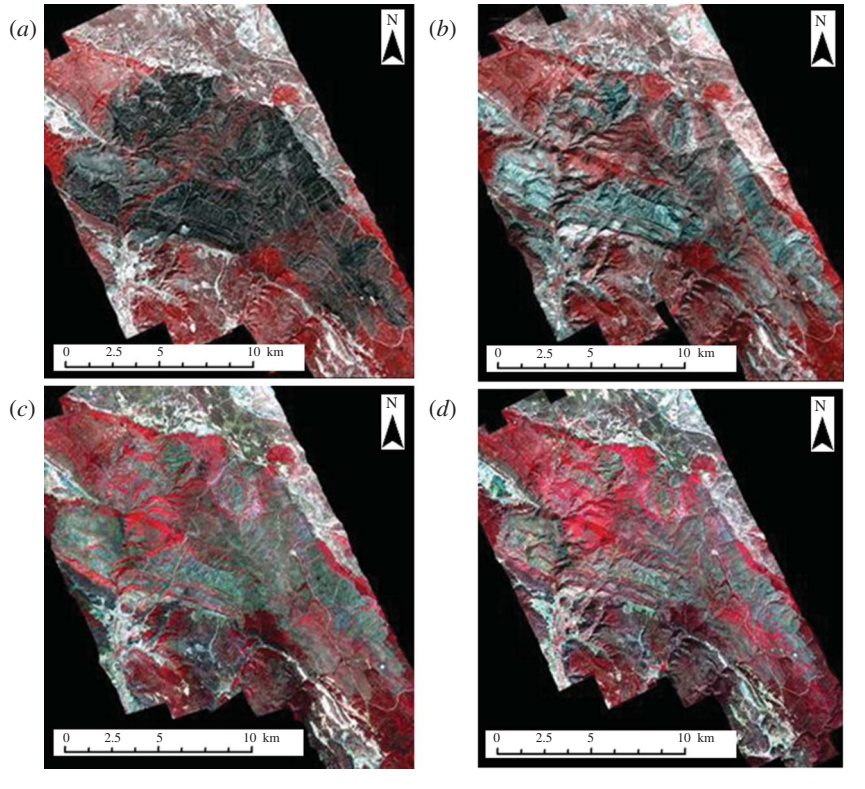

Figure 2. Hyper-spectral AHS mosaics acquired on the: (*a*) 6 October 2005; (*b*) 6 October 2006; (*c*) 28 September 2007; and (*d*) 15 September 2008.

parallel rows coinciding with the solar plane to avoid, or at least minimize, illumination problems. In addition, the flight rows overlapped, enabling the production of mosaics. Sensor and flying height were configured to produce a theoretical spatial resolution of 3.5 m. Such sensor and flight configurations were held constant for each campaign to preserve equal image acquisition conditions. Data related to flight direction and image acquisition time were also recorded to correct for the effects that different illumination geometries have on image quality.

3.2. MODIS images

MODIS images acquired by the Terra NASA (National Aeronautics and Space Administration) satellite, which was launched in 1999, were also used because of their appropriate temporal and spatial resolutions for analysing vegetation dynamics before and after fire (van Leeuwen 2008; van Leeuwen et al. 2010). In particular, the 8-day composite MOD09A1 (MODIS/Terra Surface Reflectance 8-Day L3 Global 500 m ISIN Grid version 005) surface reflectance product was selected for this study. MOD09A1 is a compound image consisting of seven surface reflectance bands located in the VIS, NIR, and SWIR regions, with bands centred at wavelengths of 648 (red), 858 (NIR), 470 (blue), 555 (green), 1240 (SWIR1), 1640 (SWIR2), and 2130 nm (SWIR3). The spatial resolution is 500 m. This product can be used to estimate the surface reflectance of each band as if it had been measured at the ground level, assuming no atmospheric distortion or absorption. A general description of the MODIS surface reflectance products can be found in the User Guide published by Vermote, Kotchenova, and Ray (2011). Using the MODIS images, we generated an NDVI time series that extends from February 2000 to December 2007. This time series was used to analyse vegetation regeneration patterns after fire at a forest state level in support of the AHS data sets with high spatial and spectral resolutions.

3.3. Ancillary data

In addition to the AHS and MODIS image data sets, we used the following ancillary information: (i) an administrative map of forest states within the study area (coordinate system: UTM Zone 30, ED-50), which was provided by the Junta de Castilla-La Mancha (Spain) (see Figure 3); (ii) data from the Second National Forest Inventory (IFN2) (ICONA 1993)

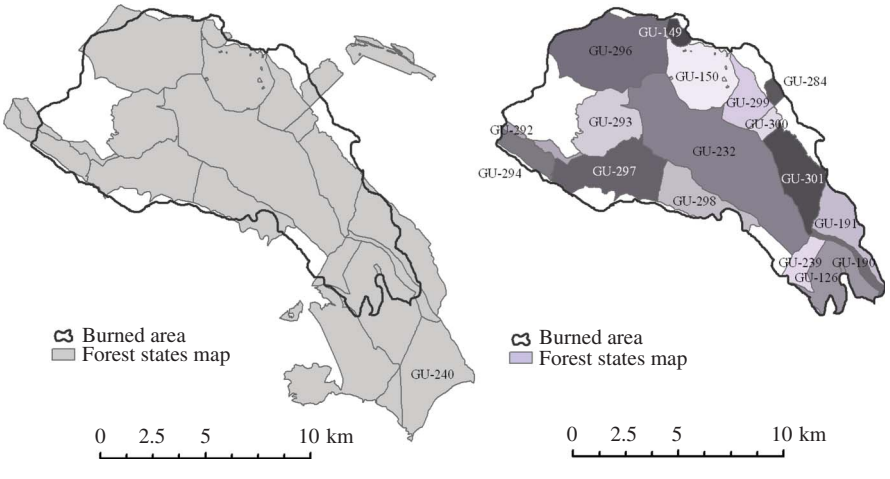

Figure 3. Forest states map and the forest states affected by the 2005 Guadalajara fire. Forest state GU-240 was not burned, so it was used as a reference sample.

for the Guadalajara province, which were provided by the Banco de Datos de la Naturaleza, Ministry of Environment (Spain); (iii) a digital elevation model at 1:25,000 scale, provided by the National Geographic Institute (coordinate system: UTM Zone 30, ED-50); and (iv) field work conducted by the Junta de Castilla-La Mancha within the study area during 2007. The administrative map was used for territorial analyses at the forest state level, while the IFN2 sample plot data were used to analyse pre-fire forest composition and structure. The digital elevation model was used for geometric corrections of the AHS images, and the field work was used for validation purposes.

4. Methodology

4.1. Fire severity field data

Three 2-day field trips were conducted in October 2005 in the study area. During the first trip, we made a general survey of the study area to plan future sampling work. Field data were collected during two subsequent trips and used to produce and validate the fire severity map that was developed from the first AHS hyper-spectral image.

Due to time limitations, the fieldwork components of this study were designed to quickly evaluate certain variables for a large area. In addition, the study area was stratified into homogeneous regions based on appropriate criteria, including vegetation type, fire severity or damage level, and accessibility. Every possible combination of fire severity and pre-fire vegetation type was registered. Sample points were categorized into two types: (i) A points, which were situated within the study area and reflected four different levels of fire severity; and (ii) B points, which were situated outside the study area (unburned sites) and were afterwards used to define training areas (endmembers) of unburned vegetation and bare soil. The coordinates of every A and B sample point were registered using a GPS device. In addition, A points were assigned to a fire severity level (unburned, low, moderate, or high), while B points were characterized by attributes such as vegetation composition, coverage percentage, structural vegetation type, height of litter, and humus (up to the mineral soil). In the laboratory, information related to the pre-fire forest vegetation condition of each of the A points was collected from the IFN2 sample plots. During the field trips, 116 A points and seven B points were collected. Fire severity levels in the field were defined according to the following criteria.

(1) Unburned (severity 0): no visible effects of fire on vegetation.
(2) Low fire severity (severity 1): less than 50% of the vegetation cover (trees plus understory) was affected by fire, and less than 30% of the trees (both dominant and co-dominant) were completely burned (in this case, shrubs and grass are the most affected).
(3) Moderate fire severity (severity 2): more than 50% and less than 90% of the vegetation cover (trees plus understory) was affected by fire, and less than 75% of the trees were completely burned (in this case, the understory is usually totally dead, although it may be capable of sprouting).
(4) High fire severity (severity 3): more than 90% of the vegetation cover (trees plus understory) appears completely burned and dead, although some species may be capable of sprouting.

4.2. Field spectra campaigns

Three field spectra campaigns were completed in the study area in 2005, 2007, and 2008, coinciding with flight times. Unfortunately, a spectra campaign was not performed in 2006.

The collected spectra were used for AHS image pre-processing (radiometric correction) and to validate the AHS correction process. According to the criteria of Che and Price (1992), field spectra data for radiometric correction and validation purposes were sampled in areas large enough to select sufficiently pure and homogeneous pixels within the image.

Field spectroscopy was conducted using an ASD Fieldspec 3 portable spectro-radiometer. This radiometer was designed to gather solar reflectance, radiance, and irradiance data in the spectral range of the VIS, NIR, and MIR regions. For radiometric correction purposes, we selected three reference surfaces: a sports field, a gravel road, and bare soil (Figure 4). For each of these surfaces, we collected three spectra series of 10 measurements each, calibrating the white spectra at the beginning of the first series and between series. In the laboratory, each series was analysed, and all out-of-range measurements were eliminated. The final spectrum for each of the three materials was the average of the three corresponding corrected series (see Figure 4).

For final product validation purposes, we selected four reference surfaces: a sports field, bare soil, a forest area, and dry grassland. For each of these surfaces, we used the procedure that was used for the three reference surfaces.

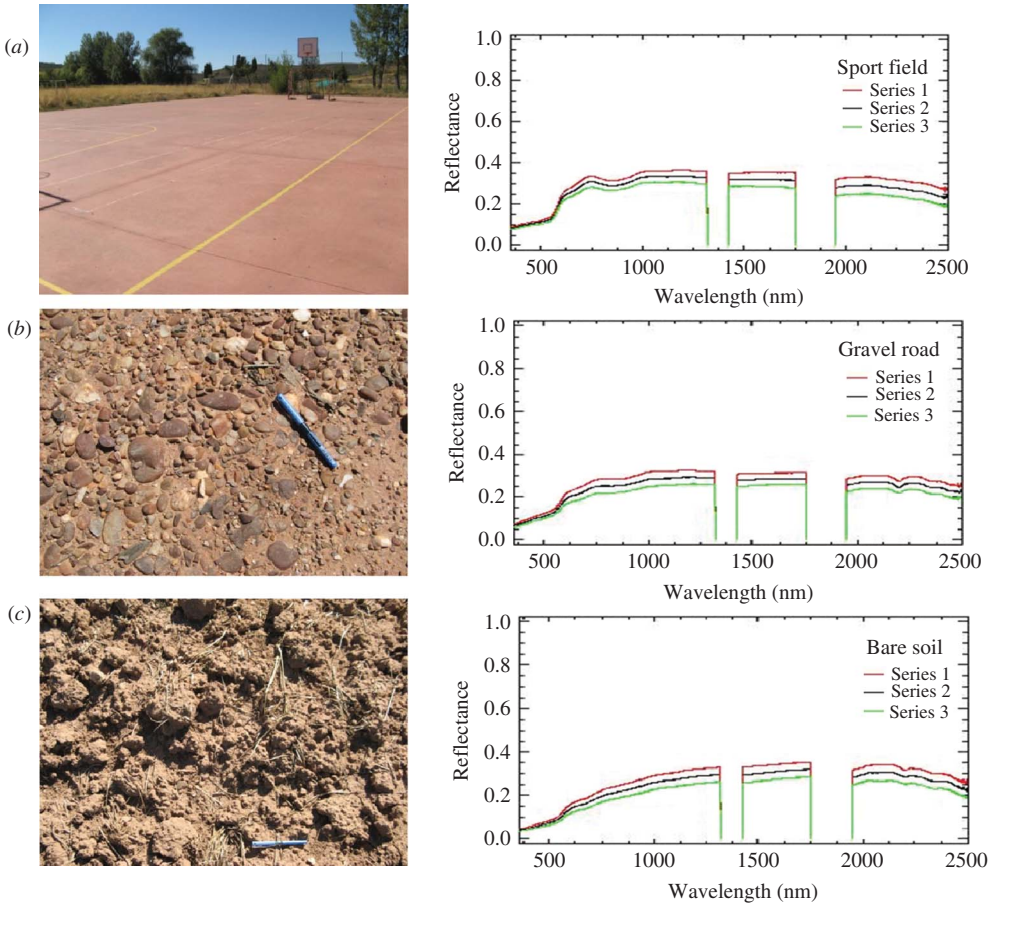

Figure 4. Field spectra campaigns reference surface pictures and spectral signatures for (*a*) a sport field, (*b*) a gravel road, and (*c*) a bare soil.

4.3. Hyper-spectral AHS images pre-processing

The raw AHS data sets were imported in binary format and stored as images. At this stage, the information content of each pixel was the digital level recorded at the time of acquisition. The pre-processing of the hyper-spectral images included the following steps: (i) radiometric correction, (ii) geometric correction, (iii) geometric multitemporal adjustment, (iv) topographic correction, (v) atmospheric correction, and (vi) reflectance multitemporal adjustment. All these steps were performed for each of the seven parallel rows that were used to generate each of the four images. This yielded 28 scenes prior to the creation of the four corresponding mosaics (one per year).

An atmospheric radiative transfer model called MODTRAN5 (Moderate Resolution Atmospheric Transmission, http://modtran5.com/, Burlington, MA, USA) was used for radiometric correction. Afterwards, PARGE (Parametric Geocoding, Wil, Switzerland; Schläpfer, Schaepman, and Itten 1998), an orthorectification and direct geocoding software for airborne optical scanner data, was used for geometric correction of the data. Both topographic and atmospheric corrections were performed with ATCOR4 (Airborne Atmospheric and Topographic Correction Model, Wil, Switzerland; Richter and Schläpfer 2002), a specific software for airborne optical scanner data. Finally, the IDL language was used to accomplish both the geometric and reflectance multitemporal adjustments. The INTA team provided support throughout these processing steps.

The pre-processing procedure started with the radiometric correction. Several sensor calibration parameters, which were calculated in the laboratory using the collected field spectra data, were used in this step. Digital levels were converted into radiances at the sensor level (top-of-atmosphere) ($W\ \mathrm{cm}^{-2}\ \mathrm{sr}^{-1}\ \mathrm{nm}^{-1}$) using the MODTRAN5 software.

Geometric corrections were then performed using the PARGE software (Schläpfer, Schaepman, and Itten 1998). The lack of stability of airborne systems introduces variations in the flight path and the attitude, which is given by the roll, pitch, and heading angles, of the plane that cannot be corrected simply with ground control points (Schläpfer, Schaepman, and Itten 1998). A pixel-by-pixel calculation must be performed instead to account for the position and altitude of the plane at the time of image acquisition (Schläpfer, Schaepman, and Itten 1998). The AHS sensor is integrated with a Flight Management System (FMS, POSTrack 410, from Applanix) that includes a GPS receiver and an inertial measurement unit (IMU). In the AHS system, synchronization is performed by sending an electronic pulse to the FMS each time a data line is acquired. Then, the FMS keeps a record that provides the position and orientation of the sensor at that particular time. A GPS reference station, which is close to the flight area, is used for differential corrections of the FMS data. The position and orientation data are then related by a Kalman filter application. As a result, the pixels are geo-located in a geodetic system of reference. Finally, the datum is transformed, and the geoid's undulation is calculated. The result is a file containing six parameters of external orientation (EO: X_{UTM}, Y_{UTM}, H_o, roll, pitch, and heading) for each AHS image line. The EO parameters are then applied to the AHS images using the PARGE software. The output is an image in which the X and Y coordinates are stored for each pixel. This file is then converted to a regular grid in which each pixel value is situated in the correct position and the rest of the grid pixels are filled using a resampling method. The IGN digital elevation model was used during the geometric correction process in the PARGE software.

In the next step, a geometric multitemporal adjustment of the four images was performed to correct positional errors introduced during the geo-referencing process. Identifying the geometric error associated with a geo-referenced image is essential to conducting an accurate analysis, especially for multitemporal studies. In this case, a

discrepancy between images can be labelled as a surface change when, in fact, it is caused by a lack of geometric accuracy between images. Therefore, to evaluate and correct any positional errors committed during the geo-referencing process, a moving window correlation method, developed by Prado Ortega (2007), was used. The result was an image in which (i) Band 1 stores the maximum correlation value found in each window, (ii) Band 2 provides the mismatches found in the X_{UTM} direction, and (iii) Band 3 provides the mismatches found in the Y_{UTM} direction, which correspond to the position of the maximum R^2 value. With the generated mismatch maps, errors were evaluated and corrected by modifying the external orientation parameters that were applied to the image. The maximum error found in this process was less than half a pixel.

The topographic correction offsets the differences in solar illumination due to altitudinal ground variations. For example, shaded areas have less reflectivity, while sunny areas have higher than expected reflectivity. The 'rugged terrain' module of the ATCOR-4 software (Airborne Atmospheric and Topographic Correction Model) (Richter and Schläpfer 2002) was used in the initial atmospheric correction step. Due to the large number of artefacts found when using this module, we decided to perform a topographic correction, using the TOPOCOR module of the ATCOR-4 software package, before applying the atmospheric correction, using the 'flat terrain' module. This approach substantially improved the results. A digital terrain model was used to obtain the elevation, slope, and aspect needed to accomplish the topographic correction. In addition, solar geometry conditions, such as the date, time, and solar zenith and azimuth angles, at the time of the flight were also taken into account.

Atmospheric corrections were performed to remove the effect of electromagnetic radiation scattering caused by gases and suspended particles in the atmosphere and to thereby produce image data that are independent of weather conditions. Further, to implement the 'flat terrain' module, several parameters were introduced to simulate the most likely atmospheric conditions: (i) the date and time of flight, the solar geometry, and the flight variables, including flight and terrain altitude, geographic direction, and solar zenith and azimuth angles; (ii) the type of sensor and calibration parameters; and (iii) the atmospheric conditions on the flight day, such as the type of aerosols and their concentrations, the level of water vapour in the air, and visibility.

To ensure a sufficient level of temporal coherence among the four hyper-spectral images, a reflectance homogenization procedure, called empirical line (Smith and Milton 1999), was performed using non-variant spectra from the 2008 field campaign. The empirical line methodology produces linear fits from 'brilliant and dark' surface spectral signatures within a study area. The surface used in this step should be invariant during the study period (2005–2008). Figure 5 shows the comparison between the spectra collected during the 2008 field campaign (spectra for validation purposes) and the spectral signatures obtained from the corrected images. As shown in Figure 5, the two spectral signatures are in agreement.

4.4. MODIS image pre-processing

MODIS products were downloaded from the NASA Distributed Active Archive Centre (DAAC, https://lpdaac.usgs.gov/) in a HDF-EOS format (Hierarchical Data Format – Earth Observation System). The MOD09A1 products were first projected into the UTM (Universal Transverse Mercator) Zone 30N – WGS-84 coordinate system using the MODIS Reprojection Tool (MRT, https://lpdaac.usgs.gov/tools/modis_reprojection_tool). NDVI was then computed for each 8-day composite, and the time series was constructed. A total of 361 images were downloaded and processed.

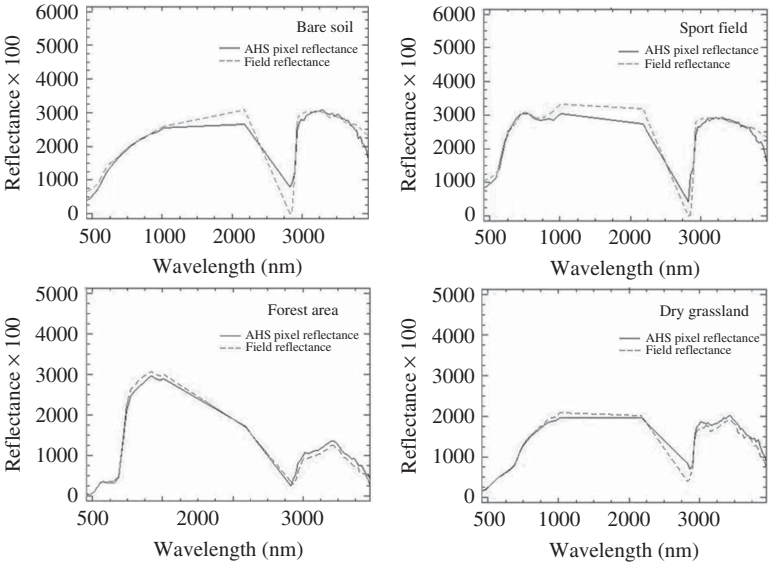

Figure 5. Spectral signatures for four ground covers (sports field, bare soil, forest area, and dry grassland) as measured in field (field reflectance) and by the AHS sensor (AHS pixel reflectance).

4.5. Image analysis

4.5.1. Burned area

After pre-processing the AHS images, the fire-affected area was delineated. The 2005 AHS image, the image that was taken closest in time to the fire event, was processed using a matched filtering analysis (Harsanyi and Chang 1994). This method assigns to a single pixel a probability value that estimates how similar the pixel is compared to an endmember collection, which is defined using a sample of 100 pixels from the AHS image itself. The resulting image was classified using an Isodata algorithm (Tou and Gonzalez 1974) to generate the final burned area map.

4.5.2. Fire severity

Fire severity was estimated using NBR (Key and Benson 2005), which has been used successfully by previous researchers (Cocke, Fulé, and Crouse 2005; Wimberly and Reilly 2007; Vicente-Serrano, Pérez-Cabello, and Lasanta 2008; Gitas, de Santis, and Mitri 2009), including those studying Mediterranean ecosystems. The NBR is calculated using pixel reflectances in the NIR and SWIR bands as shown in Equation (1):

$$\mathrm{NBR} = \frac{\rho_{\mathrm{NIR}} - \rho_{\mathrm{SWIR}}}{\rho_{\mathrm{NIR}} + \rho_{\mathrm{SWIR}}}, \tag{1}$$

where, ρ_{NIR} and ρ_{SWIR} represent surface reflectance in the NIR and SWIR bands, respectively. This spectral index was selected because it is sensible to changes in vegetation due to fire. This index varies between -1, indicating high severity, and $+1$, indicating low severity or non-affected vegetation. AHS bands for NBR calculations were selected based on low noise levels and large variabilities. According to this information, the best channel for representing NIR wavelengths was band 13, centred at 800 nm, while the suitable bands

for the SWIR wavelengths were bands 31, 38, and 41, centred at 2130, 2220, and 2250 nm, respectively. Therefore, three severity indices were calculated: NBR1, NBR2, and NBR3. An Isodata unsupervised classification method was performed to categorize fire severity into three levels of damage. One classification was performed for each of the three indices, NBR1, NBR2, and NBR3. Fire severity field data were used to select the most accurate NBR for fire severity estimation. The labelling of each spectral class to each fire severity level was done based on the NBR values, e.g. the class with lowest NBR values was associated with the highest fire severity.

Using the most accurate classification, the percentage of affected area was estimated at the forest state level with the three previously defined fire severity classes. We decided to use forest states because these are the management units used by Forest Managers. Forest states were defined using Regions of Interest (ROIs) and the cartography provided by the Junta de Castilla-La Mancha. The percentage of affected area for each severity class at the forest state level was estimated in relation to the total burned area within each state, not the total forest state area.

4.5.3. Post-fire vegetation recovery

Post-fire vegetation recovery analyses were performed using two approaches: one based on data with high spatial and spectral resolutions (AHS images) and one based on data with a high temporal resolution (MODIS time series).

The post-fire vegetation recovery assessment, based on hyper-spectral data, was conducted using a spectral unmixing procedure (Adams, Smith, and Johnson 1985), a common method for estimating the percentages of each endmember within a pixel (Settle and Drake 1993; Robichaud et al. 2007; Cochrane and Souza 1998; Smith et al. 2005). To define the spectral profile of each endmember, the Pixel Purity Index (PPI) procedure (Boardman, Kruse, and Green 1995) was applied on the minimum noise fraction (MNF) transformation (Green et al. 1988). The MNF transformation eliminates the noise in an image. In addition, the PPI is a method for selecting the purest pixels in multispectral or hyper-spectral images. Once pure pixels were selected, the inverse of the MNF was applied. The purest pixels corresponded to the basic components of the image. Finally, the pixels that clearly corresponded to full green vegetation coverage and bare soil were selected as endmembers for the spectral unmixing procedure (Figure 6).

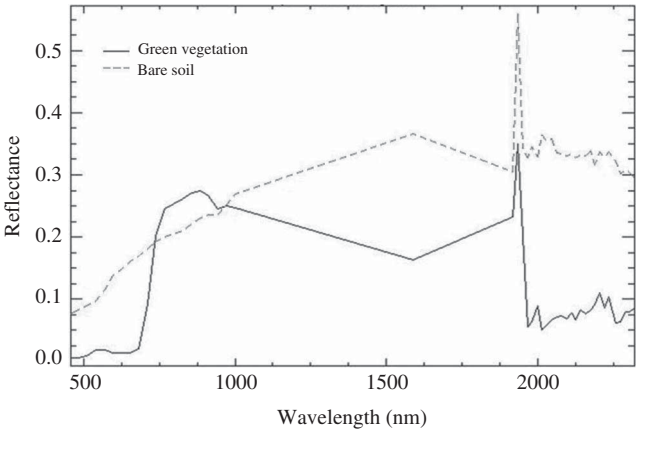

Figure 6. Green vegetation and bare soil spectral signatures.

The post-fire vegetation recovery assessment, based on the MODIS multispectral time series data, was conducted using the NDVI, which was calculated based on the red (R) and NIR reflectance values, as shown in Equation (2):

$$\mathrm{NDVI} = \frac{\rho_{\mathrm{NIR}} - \rho_{\mathrm{R}}}{\rho_{\mathrm{NIR}} + \rho_{\mathrm{R}}}, \tag{2}$$

where ρ_{R} and ρ_{NIR} represent surface reflectance in the red and NIR bands, respectively. The MODIS R and NIR bands are centred at 648 and 858 nm, respectively. This index varies between -1 and $+1$, with higher values indicating higher levels of greenness.

Average forest-state-level NDVI time series data were extracted for the temporary study of vegetation recovery. This analysis was performed to assess post-fire vegetation regeneration patterns. The time series spanned the period from February 2000 to December 2007. Pre-fire and post-fire trends were analysed in each forest state to quantitatively assess vegetation recovery. The annual pre- and post-fire vegetation patterns were also studied qualitatively.

The linear relationship between vegetation recovery estimated from the NDVI values (independent variable) for an 8-day composite period (dependent variable) was quantified. The linear equation has the following expression:

$$Y = \alpha + \beta X + \varepsilon,$$

where Y represents the NDVI values; X represents time; α is the value of the intercept; β is the slope; and ε is the error. The slope indicates regeneration intensity and whether regeneration is positive or negative.

5. Results

5.1. Burned area

Using the methodology described above, a total burned area of 129.8 km^2 was mapped (see Figure 7). This value is similar to the figure reported by the Spanish Ministry of Environment (128.8 km^2).

5.2. Fire severity

The fire severity assessment was performed using the NBR (Equation 1). Field data were used to assess the NBR-derived severity maps. The map based on NBR1 had the highest accuracy at 70%.

Figure 8 shows the spatial distribution of fire severity within the study area. In this figure, a three-level legend is used: (i) low severity (mean NBR = 0.12; 25.4 km^2 – 19.60%) is shown in white; (ii) medium severity (mean NBR = –0.20; 72.9 km^2 – 56.12%) is shown in yellow; and (iii) high severity (mean NBR = –0.37; 31.5 km^2 – 24.28%) is shown in orange. The predominant severity class is medium severity, representing approximately 72.9 km^2 (56.12%). High severity is next, representing an area of 31.5 km^2 (24.28%). Finally, low severity represents an area of 25.4 km^2 (19.60%). Figure 9 synthesizes this fire severity information based on the forest state units used by the Forest Service (Figure 3).

Table 1 shows the percentage of affected area at the forest state level, using the previously defined fire severity classes. This analysis provides an indication of the level of damage caused by the fire in each forest state.

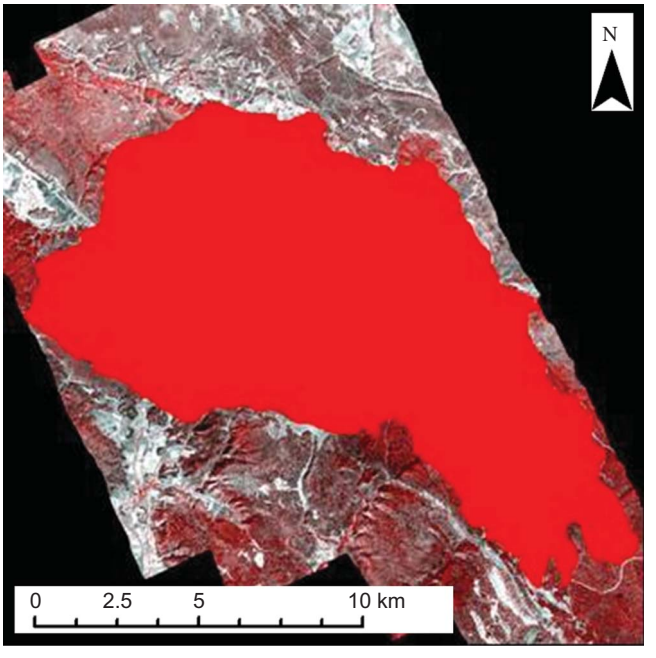

Figure 7. Burned area in red superimposed on the hyper-spectral AHS mosaic acquired on 6 October 2005.

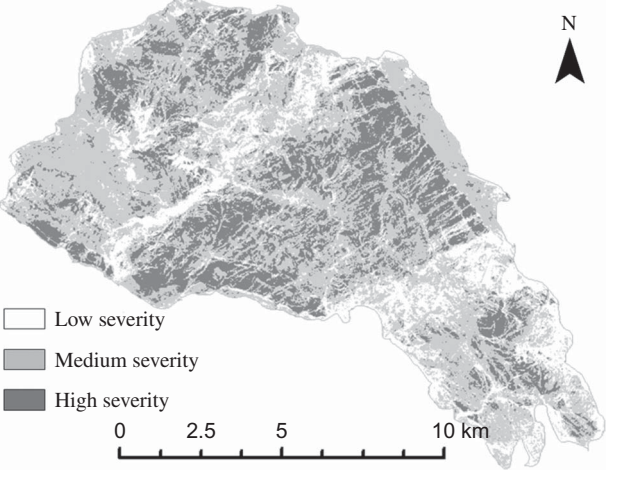

Figure 8. AHS-based fire severity map displaying three levels of damage: high, medium, and low severity.

We used forest state GU-240, in which NBR values were positive, as an unburned or non-affected forest state reference. Lower NBR values indicate higher levels of fire severity. As shown in Table 1, the forest states with the highest severity were GU-299 and GU-300, located in the central part of the study area (Figure 3). The results presented in Table 1 show that in these forest states, more than half of the affected area was classified as high severity.

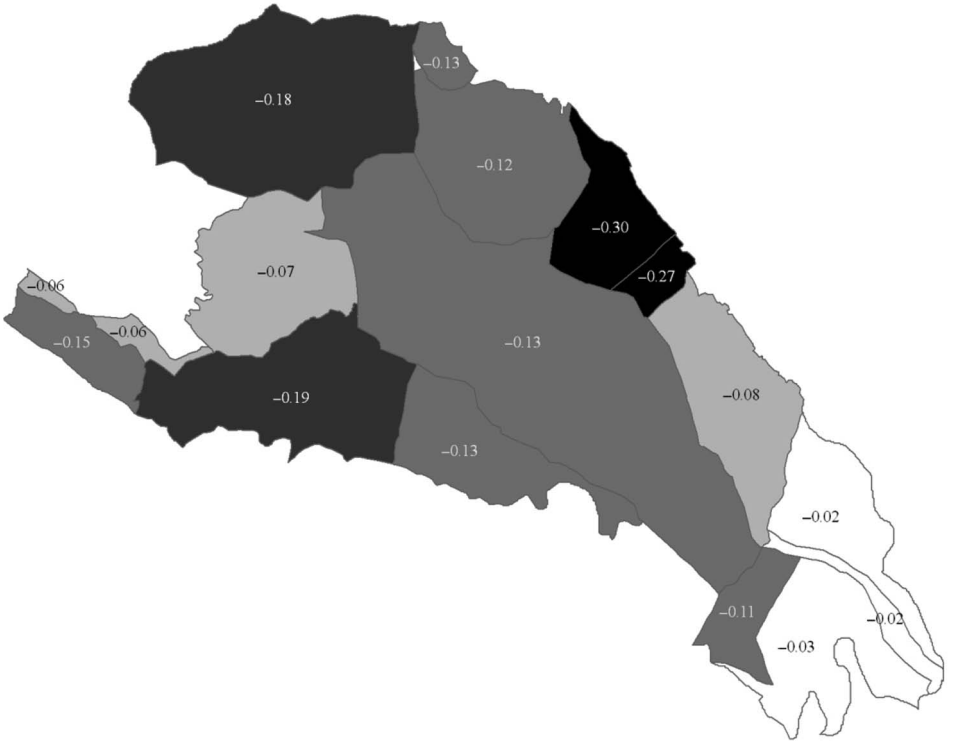

Figure 9. Mean AHS-derived fire severity value, estimated using the NBR and calculated at the forest state level. The highest severity level is dark grey, while the lowest level is white.

Table 1. AHS-derived burned area (in per cent) as a function of fire severity.

ID	Name (municipality)	High severity (%)	Medium severity (%)	Low severity (%)
GU-126	Dehesa Común (Cobeta)	14.92	53.69	31.39
GU-149	Dehesa (Ciruelos del Pinar)	17.19	70.45	12.36
GU-150	Pinar (Ciruelos del Pinar)	18.32	54.82	26.86
GU-190	Entredicho (Selas)	9.23	53.50	37.27
GU-191	El Pinar (Selas)	13.48	36.42	50.10
GU-232	Dehesa Común de Solanillos (Mazarete)	23.07	59.33	17.60
GU-239	Los Casares (Cobeta)	19.61	64.06	16.33
GU-292	Sierra del Gallubar y Vigorra, Los Milagros, Vallejo del Cabrero y las Ocecillas (Anguita)	17.34	53.23	29.43
GU-293	El Bosque del Buen Desvío (Anguita)	16.53	54.06	29.41
GU-294	El Pinar (Anguita)	27.44	63.62	8.95
GU-296	Pinar (Luzón)	33.00	55.97	11.03
GU-297	La Tasuguera (Riba de Saelices)	42.36	45.29	12.36
GU-298	Ceño Negrillo y la Virgen (Ablanque)	29.52	50.71	19.77
GU-299	El Pinar (Mazarete)	63.38	35.55	1.08
GU-300	El Pinarejo (Anquela del Ducado)	56.15	41.54	2.31
GU-301	Dehesa de la Mata (Anquela del Ducado)	26.89	38.49	34.62

Forest states GU-190, GU-191, and GU-126 had the lowest NBR values. They are situated in the southeast part of the study area, near GU-240, the non-affected forest state. In these forest states, more than half of the affected area is classified as medium or low severity.

5.3. *Post-fire vegetation recovery using AHS images*

The evolution of vegetation during the period from 2005 to 2008 was assessed using the spectral unmixing procedure (Figure 10). The light grey areas represent high levels of vegetation coverage, while dark grey areas are those where either the percentage of bare soil is high or the vegetation coverage is low.

Table 2 presents the average vegetation cover at the forest state level. The results show that the areas with the highest degree of vegetation recovery are located in the northwest, while those with the lowest amount of vegetation recovery are located in the southeast. Forest states 'Dehesa' (GU149), 'El Bosque del Buen Desvío' (GU293), and 'Pinar' (GU296), all of which are located in the northwest section of the affected area, had the greatest regeneration rates. Forest state GU298, located in the central part of the study area, had the lowest rate of regeneration. Forest states GU126, GU191, and GU-190, all of which are in the southeast, also had low levels of regeneration. The field work conducted by the Junta de Castilla-La Mancha during 2007 and expert opinions confirm the precision of these regeneration maps.

5.4. *Post-fire vegetation recovery using MODIS time series*

Figure 11 shows the temporal evolution of the MODIS NDVI time series for each forest state between February 2000 and December 2007. All the series clearly show the effect of

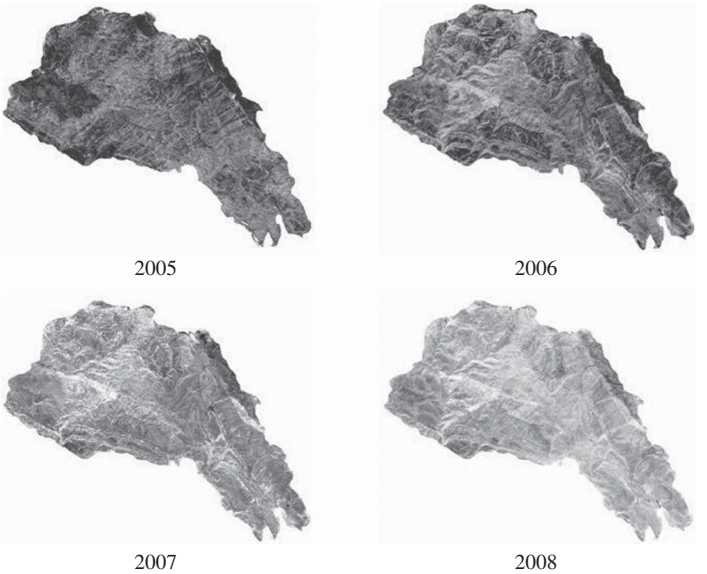

Figure 10. AHS-derived green coverage percentage, estimated from spectral unmixing in 2005, 2006, 2007, and 2008. Grey scale ranges from black, representing bare soil, to white, representing full vegetation coverage.

Table 2. Mean percentage of vegetation cover per forest state resulting from the spectral unmixing procedure based on AHS hyper-spectral images.

	% Vegetation cover			
ID	2005	2006	2007	2008
GU-126	0.17	0.32	0.32	0.33
GU-149	0.17	0.59	0.66	0.52
GU-150	0.13	0.29	0.32	0.36
GU-190	0.17	0.26	0.23	0.31
GU-191	0.17	0.24	0.19	0.32
GU-232	0.12	0.29	0.26	0.34
GU-239	0.12	0.29	0.31	0.33
GU-292	0.09	0.15	0.25	0.34
GU-293	0.15	0.43	0.53	0.44
GU-294	0.08	0.22	0.29	0.33
GU-296	0.09	0.31	0.38	0.38
GU-297	0.06	0.21	0.28	0.32
GU-298	0.10	0.19	0.18	0.30
GU-299	0.05	0.28	0.23	0.33
GU-300	0.04	0.21	0.21	0.31
GU-301	0.13	0.24	0.22	0.32

the fire event in the vegetation response, as measured by the satellite. Figure 11 also shows the NDVI time series trend in the pre- and post-fire conditions.

During the pre-fire stage, forest states GU-296, GU-293, and GU-149 showed a sharp increase in the NDVI values at the beginning of spring, followed by a smooth decrease in vegetation greenness during the dry period. However, for the other forest states, the opposite pattern was observed. At the beginning of spring, the NDVI values increased gradually and then decreased sharply during the dry season. The pre-fire vegetation trend showed a value near zero.

Coinciding with the fire event, a sharp drop in the NDVI values was observed in all cases as a result of the drastic reduction in vegetation greenness caused by fire. After the pre-fire vegetation patterns were analysed, the temporal evolution of vegetation in each forest state was evaluated for the following years (Table 3). The trend analysis yielded different slope values, or vegetation recovery rates, for each forest state.

The vegetation pattern of forest states GU-149, GU-293, and GU-296 during the first year after the fire followed two cycles (Figure 11(*a*)). However, during 2007, the pattern changed from a bimodal pattern to a unimodal pattern, with a maximum value in spring and a minimum value in fall–winter. Further, comparing the pre- and post-fire patterns revealed many similarities. The trend analysis showed a positive slope in the curve, indicating a positive trend in the regeneration process. Forest states GU-294 and GU-297 presented an irregular pattern (Figure 11(*b*)) during the post-fire period. The NDVI values increased from July 2005 to December 2007 following a period of irregular temporal behaviour. The vegetation recovery model indicated a low positive trend for GU-294. During the first year after the fire, forest states GU-150, GU-232, GU-239, and GU-301 (Figure 11(*c*)) showed patterns similar to forest states GU-149, GU-293, and GU-296. These patterns were characterized by a marked double cycle. The vegetation recovery model showed positive slope values for GU-232 and GU-239, whereas for GI-150 and GU-301, the trend analysis showed low values. Forest states GU-299 and GU-300 showed clear increases in the NDVI values during the years after the fire, with maximum values above 0.5 (Figure 11(*d*)).

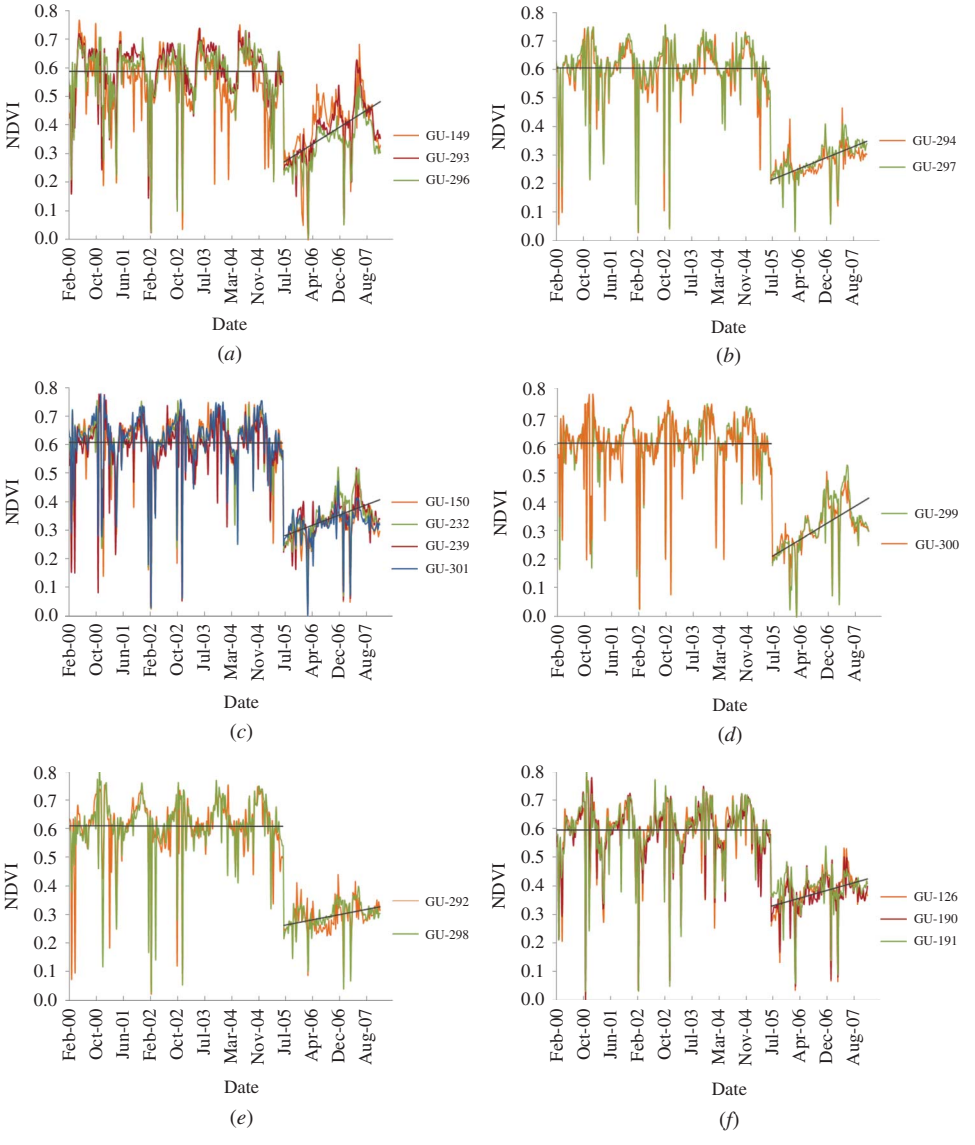

Figure 11. MODIS-derived NDVI temporal evolution estimated during the period 2000–2007 at the forest state level: (*a*) GU-149, GU-293, and GU-296; (*b*) GU-294 and GU-297; (*c*) GU-150, GU-232, GU-239, and GU-301; (*d*) GU-299 and GU-300; (*e*) GU-292 and GU-296; and (*f*) GU-126, GU-190, and GU-191.

However, a double cycle was observed in 2007. The vegetation recovery model showed positive values for both forest states. The patterns observed in forest states GU-292 and GU-298 were irregular during the first year after the fire, followed by a double cycle pattern in subsequent years (Figure 11(*e*)). The vegetation recovery analysis yielded slope values near zero. During the post-fire period, forest states GU-126, GU-190, and GU-191 (Figure 11(*f*)) showed no significant increases in the NDVI values, and the trend analysis showed low slope values near zero.

Table 3. Average NDVI as derived from MODIS time series during the pre-fire period and after fires in 2006 and 2007. NDVI was scaled from 0 (bare soil) to 1 (full vegetation cover).

	GU-149 GU-293 GU-296	GU-294 GU-297	GU-150 GU-232 GU-239 GU-301	GU-299 GU-300	GU-292 GU-298	GU-126 GU-190 GU-191
NDVI pre-fire	0.569	0.598	0.606	0.603	0.609	0.592
NDVI 2006	0.365	0.261	0.323	0.298	0.282	0.375
NDVI 2007	0.409	0.305	0.348	0.356	0.308	0.386

Table 3 summarizes the mean NDVI values during the pre-fire period from February 2000 until the date of the fire. This table also shows the mean NDVI values during the post-fire period for the years 2006 and 2007.

These results show the similarity of the NDVI values in most of the forest states during the pre-fire period, with values ranging from 0.57 to 0.60. As a result of the fire, the NDVI values decreased to approximately 0.30 in all forest states except GU-126 and GU-190, where the values fell to 0.20. In 2007, a maximum difference of 0.1 was observed among forest states.

6. Discussion

Vegetation recovery studies based on remotely sensed data are often based on multispectral data with medium to high spatial resolutions (Viedma et al. 1997; Miller and Yool 2002; Díaz-Delgado, Lloret, and Pons 2003; Lentile et al. 2006; Röder et al. 2008; Vicente-Serrano, Pérez-Cabello, and Lasanta 2008), though several studies have used hyper-spectral data with high spatial and spectral resolutions (Riaño et al. 2002). However, the lack of temporal continuity, including the non-availability of pre-fire information, and the high cost of these images complicate their use. Recently, sensors such as MODIS, which produce data with a high temporal resolution and extent, have been used for vegetation recovery analysis on broad scales (Van Leeuwen 2008; van Leeuwen et al. 2010).

In this research, we combined hyper-spectral AHS information with multitemporal long-term MODIS time series data to better understand post-fire vegetation recovery. AHS data were used to determine the amount of green vegetation at a sub-pixel level, while MODIS data were used to assess the temporal patterns of vegetation types that clearly indicate regeneration. The percentage of vegetation cover over time generally indicates regeneration in a given area, but this process should be extended to account for other factors, such as post-fire vegetation patterns and fire severity.

The AHS-based regeneration maps reveal vegetation recovery during the 4-year post-fire study period. According to the results from the 2007 field surveys, the highest levels of vegetation recovery occurred in areas with a predominance of *Quercus* sp. and shrubs because these species actively re-sprout. The lowest levels of vegetation recovery occurred in areas with no regeneration or with a predominance of *Pinus* sp. In this case, differentiating between vegetation recovery and bare soil was difficult because the percentage of bare soil within pixels was high during the first recovery stages, as *Pinus pinaster* regenerates from seed.

Before the fire, forest states GU-149, GU-293, and GU-296 showed a sharp increase in the NDVI values at the beginning of spring, likely coinciding with the emergence of leaves on deciduous species. During the dry period, a smooth decrease in the NDVI values was

observed, likely as a result of the loss of moisture at the beginning and the eventual falling of leaves. The opposite pattern was observed in the other forest states; at the beginning of spring, the NDVI values increased gradually due to the mixture of herbs, shrubs, and evergreens, while during the dry season, the NDVI values declined sharply due to the rapid drying of the herbaceous vegetation.

During the post-fire stage, forest states GU-149, GU-293, and GU-296 had higher regeneration rates, mainly due to the regeneration of *Quercus pyrenaica,* the dominant species in these areas. The forest states with the lowest regeneration rates, GU-126, GU-190, and GU-191, are located in the south. These areas showed moderate levels of *Pinus pinaster* regeneration during the 2007 field work; therefore, the poor AHS-based regeneration rates found in these forests may be due to the high proportion of bare soil associated with pine regeneration.

The double cycle observed in forest states GU-149, GU-293, and GU-296 after the fire is characteristic of herbaceous species. In this case, the NDVI values increase during the spring as a result of photosynthetic activity and gradually decline during the summer due to the loss of vegetation moisture. During the fall, another NDVI increase was observed, coinciding with the emergence of herbaceous species prompted by rainfall. However, throughout 2007, the pattern changed from bimodal to unimodal, a trend similar to the pre-fire vegetation response. Although the post-fire NDVI values are lower than the pre-fire values, we concluded that no management practices were needed in these forest states. The same situation was observed for forest states GU-150, GU-232, GU-239, and GU-301.

Forest states GU-299 and GU-300 showed clear increases in the NDVI values during the subsequent post-fire years, reaching values above 0.5. This result could indicate a high level of forest regeneration. However, after analysing this pattern in more detail, a double cycle was identified. This cycle was still present in 2007. This double cycle is characteristic of herbaceous vegetation, which could indicate low rates of forest regeneration. Therefore, these forest states may be selected for immediate intervention.

The irregular pattern observed during the first post-fire year in forest states GU-298 and GU-292 and the double cycle pattern observed during the next years could indicate either a low rate of regeneration or the dominance of shrubs and herbaceous vegetation. The increase of greenness during the post-fire period was significantly low, which could indicate a lack of regeneration and, thus, the need for immediate intervention in these states. A similar situation was observed in forest states GU-294 and GU-297.

The increase of the NDVI values in forest states GU-126, GU-190, and GU-191 during the post-fire period was not significantly high. However, based on changes during the pre-fire period, the decrease of the NDVI values was also not as severe as in other forest states. Thus, although the NDVI increase in these states was lower during the post-fire period than in the other affected forest states, the NDVI value was near 0.5, indicating the gradual recovery of vegetation in these forest states.

7. Conclusions

Following a forest fire, the most important data sets are maps of the affected area and estimates of the level of damage caused by the fire. Monitoring vegetation recovery in the subsequent years is also valuable. These three types of information are key aspects in forest planning and management. This study demonstrated how the high spectral quality and spatial resolution of hyper-spectral data can be combined with the high temporal resolution of multispectral data to monitor vegetation recovery.

Compared to the official figures from the Ministry of Environment, the AHS hyper-spectral images accurately mapped fire affected areas; the AHS images yielded an area of 129.8 km^2, while the Ministry's statistics reported an area of 128.9 km^2. This result confirms our hypothesis regarding the ability of hyper-spectral images to provide the cartography of burned areas.

The AHS hyper-spectral images also yielded accurate estimates of fire severity (i.e. the level of damage). The NBR1 data provided a highly accurate severity index. This result further corroborates the utility of remote sensing in estimating damage after a forest fire.

Finally, the AHS hyper-spectral images yielded reasonably accurate estimates of the degree of post-fire vegetation recovery, especially in areas dominated by *Quercus* sp. and shrubs. Combining hyper-spectral vegetation recovery images with multitemporal MODIS data and fire severity cartography provides a better understanding of post-fire vegetation recovery patterns. Based on this multi-source analysis, areas in need of urgent interventions can be identified, thus facilitating post-fire management practices in the affected area.

The types of information used in this study provide forest managers with a reliable, fast, and economical tool compared to traditional methods such as field work.

Acknowledgements

This research was conducted as part of a collaboration agreement between INIA and the Junta de Comunidades de Castilla – La Mancha (code: CC0621). The authors thank the Forest Service in Guadalajara for the support offered during visits to the study area and for assistance with fieldwork. The authors also thank the Remote Sensing Laboratory of the INTA (Spain) for their help with pre-processing the AHS images.

References

Adams, J. B., M. O. Smith, and P. E. Johnson. 1985. "Spectral Mixture Modeling: A New Analysis of Rock and Soil Types at the Viking Lander 1 Site." *Journal of Geophysical Research* 91 (B8): 8098–8112.

Boardman, J. W., F. A. Kruse, and R. O. Green. 1995. "Mapping Target Signatures via Partial Unmixing of AVIRIS Data." Paper presented at the Fifth Annual JPL Airborne Earth Science Workshop, Pasadena, CA, January 23–26.

Che, N., and J. C. Price. 1992. "Survey of Radiometric Calibration Results and Methods for Visible and Near Infrared Channels of NOAA-7, -9, and -11 AVHRRs." *Remote Sensing of Environment* 41 (1): 19–27.

Chuvieco, E. 2009. "Global Impacts of Fire." In *Earth Observation of Wildland Fires in Mediterranean Ecosystems*, edited by E. Chuvieco, 1–10. Berlin: Springer.

Cochrane, M. A., and C. M. Souza. 1998. "Linear Mixture Model Classification of Burned Forests in the Eastern Amazon." *International Journal of Remote Sensing* 19 (17): 3433–3440.

Cocke, A. E., P. Z. Fulé, and J. E. Crouse. 2005. "Comparison of Burn Severity Assessments Using Differenced Normalized Burn Ratio and Ground Data." *International Journal of Wildland Fire* 14 (2): 189–198.

De Santis, A., and E. Chuvieco. 2007. "Burn Severity Estimation from Remotely Sensed Data: Performance of Simulation versus Empirical Models." *Remote Sensing of Environment* 108 (4): 422–435.

Díaz-Delgado, R., F. Lloret, and X. Pons. 2003. "Influence of Fire Severity on Plant Regeneration through Remote Sensing Imagery." *International Journal of Remote Sensing* 24 (8): 1751–1763. doi:10.1080/01431160210144732.

Drake, N. A., S. Mackin, and J. J. Settle. 1999. "Mapping Vegetation, Soils, and Geology in Semiarid Shrublands Using Spectral Matching and Mixture Modeling of SWIR AVIRIS Imagery." *Remote Sensing of Enviornment* 68 (1): 12–25.

Gitas, I. Z., A. de Santis, and G. H. Mitri. 2009. "Remote Sensing of Burn Severity." In *Earth Observation of Wildland Fires in Mediterranean Ecosystems*, edited by E. Chuvieco, 129–148 Berlin: Springer.

González-Alonso, F., S. Merino-de-Miguel, A. Roldán-Zamarrón, S. García-Gigorro, and J. M. Cuevas. 2007. "MERIS Full Resolution Data for Mapping Level-of-Damage by Forest Fires: The Valencia De Alcántara Event in August 2003." *International Journal of Remote Sensing* 28 (3–4): 797–809.

Green, A. A., M. Berman, P. Switzer, and M. D. Craig. 1988. "A Transformation for Ordering Multispectral Data in Terms of Image Quality with Implications for Noise Removal." *IEEE Transactions on Geoscience and Remote Sensing* 26 (1): 65–74.

Harsanyi, J. C., and C. Chang. 1994. "Hyperspectral Image Classification and Dimensionality Reduction: An Orthogonal Subspace Projection Approach." *IEEE Transactions on Geoscience and Remote Sensing* 32 (4): 779–785.

ICONA. 1993. *Segundo Inventario Forestal Nacional. Guadalajara. 1986–1995*. Madrid: Ministerio de Agricultura, Pesca y Alimentación.

Key, C. H., and N. C. Benson. 2005. "Landscape Assessment: Remote Sensing of Severity, the Normalized Burn Ratio." In *FIREMON: Fire Effects Monitoring and Inventory System*, edited by D. C. Lutes. Ogden: USDA Forest Service, Rocky Mountain Research Station.

Kokaly, R. F., B. W. Rockwell, S. L. Haire, and T. V. V. King. 2007. "Characterization of Post-Fire Surface Cover, Soils and Burn Severity at the Cerro Grande Fire, New Mexico, Using Hyperspectral and Multispectral Remote Sensing." *Remote Sensing of Environment* 106 (3): 305–325.

Lentile, L. B., Z. A. Holden, A. M. S. Smith, M. J. Falkowski, A. T. Hudak, P. Morgan, S. A. Lewis, P. E. Gessler, and N. C. Benson. 2006. "Remote Sensing Techniques to Assess Active Fire Characteristics and Post-Fire Effects." *International Journal of Wildland Fire* 15 (3): 319–345.

Lentile, L. B., A. M. S. Smith, A. T. Hudak, P. Morgan, M. J. Bobbitt, S. A. Lewis, and P. R. Robichaud. 2009. "Remote Sensing for Prediction of 1-Year Post-Fire Ecosystem Condition." *International Journal of Wildland Fire* 18 (5): 594–608.

Levine, J. S. 1991. "Introduction." In *Global Biomass Burning: Atmospheric, Climatic and Biospheric Implications*, edited by J. S. Levine. Cambridge, MA: MIT Press.

Levine, J. S. 1996. "Introduction." In *Biomass Burning and Global Change: Remote Sensing, Modeling and Inventory Development, and Biomass Burning in Africa*, edited by J. S. Levine. Cambridge, MA: MIT press.

Lewis, S. A., L. B. Lentile, A. T. Hudak, P. R. Robichaud, P. Morgan, and M. J. Bobbitt. 2007. "Mapping Ground Cover Using Hyperspectral Remote Sensing after the 2003 Simi and Old Wildfires in Southern California." *Fire Ecology* 3 (1): 109–128.

Miller, A. B., and S. R. Yool. 2002. "Mapping Forest Post-Fire Canopy Consumption in Several Overstory Types Using Multi-Temporal Landsat TM and ETM Data." *Remote Sensing of Environment* 82 (2–3): 481–496.

Miller, J. D., and A. E. Thode. 2007. "Quantifying Burn Severity in a Heterogeneous Landscape with a Relative Version of the Delta Normalized Burn Ratio (dNBR)." *Remote Sensing of Environment* 109 (1): 66–80.

Mooney, H. A., and R. J. Hobbs. 1986. "Resillience at the Individual Plant Level." In *Resillience in Mediterranean-Type Ecosystems*, edited by B. B. Dell, D. Lamont, and A. J. Hopkins, 65–82. The Hague: Dr. W. Junk.

Moreno, J. M. 2007. "Cambio global e incendios forestales: Una visión desde España." Paper presented at the 4th Wildfire International Conference, Sevilla, May 10–14.

Palacios-Orueta, A., E. Chuvieco, A. Parra, and C. Carmona-Moreno. 2005. "Biomass Burning Emissions: A Review of Models Using Remote-Sensing Data." *Environmental Monitoring and Assessment* 104 (1–3): 189–209.

Pausas, J. G. 2004. "Changes in Fire and Climate in the Eastern Iberian Peninsula (Mediterranean Basin)." *Climatic Change* 63: 337–350.

Pausas, J. G., E. Ribeiro, and R. Vallejo. 2004. "Post-Fire Regeneration Variability of *Pinus Halepensis* in the Eastern Iberian Peninsula." *Forest Ecology and Management* 203 (1–3): 251–259.

Pérez-Cabello, F., M. T. Echeverría, P. Ibarra, and J. de la Riva. 2009. "Effects of Fire on Vegetation, Soil and Hydrogeomorpholocial Behavior in Mediterranean Ecosystems." In *Earth Observation of Wildland Fires in Mediterranean Ecosystems*, edited by E. Chuvieco, 111–128. Berlin: Springer.

Prado Ortega, E. 2007. "Mejoras en la evaluación y corrección de errores de corregistro en imágenes hiperspectrales AHS para estudios multitemporales." Master's thesis, Universidad de Alcalá de Henares, Madrid, España.

Retana, J., J. M. Espelta, A. Habrouk, J. L. Ordoñez, and F. Solà-Morales. 2002. "Regeneration Patterns of Three Mediterranean Pines and Forest Changes after a Large Wildfire in Northeastern Spain." *Ecosience* 9 (1): 89–97.

Riaño, D., E. Chuvieco, S. Ustin, R. Zomer, P. Dennison, D. Roberts, and J. Salas. 2002. "Assessment of Vegetation Regeneration after Fire through Multitemporal Analysis of AVIRIS Images in the Santa Monica Mountains." *Remote Sensing of Environment* 79 (1): 60–71.

Richter, R., and D. Schläpfer. 2002. "Geo-Atmospheric Processing of Airborne Imaging Spectrometry Data. Part 2: Atmospheric/Topographic Correction." *International Journal of Remote Sensing* 23 (13): 2631–2649.

Robichaud, P. R., S. A. Lewis, D. Y. M. Laes, A. T. Hudad, R. F. Kokaly, and J. A. Zamudio. 2007. "Postfire Soil Burn Severity Mapping with Hyperspectral Image Unmixing." *Remote Sensing of Environment* 108 (4): 467–580.

Röder, A., J. Hill, B. Duguy, J. A. Alloza, and R. Vallejo. 2008. "Using Long Time Series of Landsat Data to Monitor Fire Events and Post-Fire Dynamics and Identify Driving Factors. A Case Study in the Ayora Region (Eastern Spain)." *Remote Sensing of Environment* 112 (1): 259–273.

Roldán-Zamarrón, A., S. Merino-de-Miguel, F. González-Alonso, S. García-Gigorro, and J. M. Cuevas. 2006. "Minas De Riotinto (South Spain) Forest Fire: Burned Area Assessment and Severity Mapping Using Landsat 5 – TM, Envisat – MERIS and Terra – MODIS Post-Fire Images." *Journal of Geophysical Research* 111: G04S11.

Roy, D. P., L. Boschetti, and S. N. Trigg. 2006. "Remote Sensing of Fire Severity: Assessing the Performance of the Normalized Burn Ratio." *IEEE Geoscience and Remote Sensing Letters* 3 (1): 112–116. doi:10.1109/LGRS.2005.858485.

Ruíz-Gallardo, J. R., S. Castaño, and A. Calera. 2004. "Application of Remote Sensing and GIS to Locate Priority Intervention Areas after Wildland Fires in Mediterranean Systems: A Case Study From South-Eastern Spain." *International Journal of Wildland Fire* 13 (3): 241–252. doi:10.1071/WF02057.

Schläpfer, D., M. E. Schaepman, and K. I. Itten. 1998. "PARGE: Parametric Geocoding Based on GCP-Calibrated Auxiliary Data." *Imaging Spectrometry IV SPIE* 3438: 334–344.

Settle, J. J., and N. A. Drake. 1993. "Linear Mixing and the Estimation of Ground Cover Proportions." *International Journal of Remote Sensing* 14 (6): 1159–1177.

Smith, A. M. S., M. J. Wooster, N. A. Drake, F. M. Dipotso, M. J. Falkowski, and A. T. Hudak. 2005. "Testing the Potential of Multi-Spectral Remote Sensing for Retrospectively Estimating Fire Severity in African Savannahs." *Remote Sensing of Environment* 97 (1): 92–115.

Smith, G. M., and E. J. Milton. 1999. "The Use of the Empirical Line Method to Calibrate Remotely Sensed Data to Reflectance." *International Journal of Remote Sensing* 20 (13): 2653–2662.

Tou, J. T., and R. C. González. 1974. *Pattern Recognition Principles*. Reading, MA: Addison-Wesley Publishing Company.

Van der Werf, G. R., J. T. Randerson, L. Gilgio, G. J. Collatz, M. Mu, P. S. Kasibhatla, D. C. Morton, R. S. DeFries, Y. Jin, and T. T. van Leeuwen. 2010. "Global Fire Emissions and the Contribution of Deforestation, Savanna, Forest, Agricultural, and Peat Fires (1997–2009)." *Atmospheric Chemistry and Physics* 10: 11707–11735. doi:10.51194/acp-10-11707–2010.

van Leeuwen, W. J. D. 2008. "Monitoring the Effects of Forest Restoration Treatments on Post-Fire Vegetation Recovery with MODIS Multitemporal Data." *Sensors* 8 (3): 2017–2042. doi:10.3390/S8032017.

van Leeuwen, W. J. D., G. M. Casady, D. G. Neary, S. Bautista, J. A. Alloza, Y. Carmel, L. Wittenberg, D. Malkinson, and B. J. Orr. 2010. "Monitoring Post-Wildfire Vegetation Response with Remotely Sensed Time-Series Data in Spain, USA and Israel." *International Journal of Wildland Fire* 19 (1): 75–93.

Vermote, E. F., S. Y. Kotchenova, and J. P. Ray. 2011. "MODIS Surface Reflectance User's Guide." Accessed February 21, 2012. http://modis-sr.ltdri.org/products/MOD09_UserGuide_v1_3.pdf.

Vicente-Serrano, S., F. Pérez-Cabello, and T. Lasanta. 2008. "Assessment of Radiometric Correction Techniques in Analyzing Vegetation Variability and Change Using Time Series of Landsat Images." *Remote Sensing of Environment* 112 (10): 3916–3934.

Viedma, O., J. Meliá, D. Segarra, and J. García-Haro. 1997. "Modeling Rates of Ecosystem Recovery after Fires by Using Landsat TM Data." *Remote Sensing of Environment* 61 (3): 383–398.

White, J. D., K. C. Ryan, C. Key, and S. W. Running. 1996. "Remote Sensing of Forest Fire Severity and Vegetation Recovery." *International Journal of Wildland Fire* 6 (3): 125–136.

Wimberly, M. C., and M. J. Reilly. 2007. "Assessment of Fire Severity and Species Diversity in the Southern Appalachians Using Landsat TM and ETM+ Imagery." *Remote Sensing of Environment* 108 (2): 189–197.